Chinese Chemical Letters 36 (2025) 110212

Contents lists available at ScienceDirect

Chinese Chemical Letters

journal homepage: www.elsevier.com/locate/cclet

MMP-9-responsive probe for fluorescence-magnetic resonance dual-mode imaging of hepatocellular carcinoma models with different metastatic capacities

Qiuye Wang[a,1], Yabing Sun[a,b,1], Liangxue Lai[a,b], Haijing Cui[a,b], Yonglong Ye[a], Ming Yang[a], Weihao Zhu[a,b], Bo Yuan[a,c], Quanliang Mao[d], Wenzhi Ren[a,b,c,*], Aiguo Wu[a,c,*]

[a] *Ningbo Key Laboratory of Biomedical Imaging Probe Materials and Technology, Zhejiang International Cooperation Base of Biomedical Materials Technology and Application, Chinese Academy of Sciences (CAS) Key Laboratory of Magnetic Materials and Devices, Ningbo Cixi Institute of Biomedical Engineering, Zhejiang Engineering Research Center for Biomedical Materials, Ningbo Institute of Materials Technology and Engineering, Chinese Academy of Sciences, Ningbo 315201, China*

[b] *Cixi Biomedical Research Institute, Wenzhou Medical University, Ningbo 315300, China*

[c] *Advanced Energy Science and Technology Guangdong Laboratory, Huizhou 516000, China*

[d] *Department of Radiology, First Affiliated Hospital of Ningbo University, Ningbo 315010, China*

ARTICLE INFO

Article history:
Received 13 April 2024
Revised 25 June 2024
Accepted 3 July 2024
Available online 3 July 2024

Keywords:
Hepatocellular carcinoma
Matrix metalloproteinase-9
Fluorescence imaging
Magneticresonance imaging
Förster resonance energy transfer

ABSTRACT

Visual assessment of tumor metastatic capacity is crucial for predicting hepatocellular carcinoma (HCC) prognosis and guiding clinical therapeutic approaches. In this study, we developed an enzyme-responsive probe based on the peptide GK10, which is selectively cleaved by matrix metalloproteinase-9 (MMP-9), a critical marker for metastasis in HCC. The GK10 peptide was conjugated with near-infrared fluorescent molecule IR783, fluorescent quencher black hole quencher 3 (BHQ3), and magnetic resonance (MR) contrast agent DOTA-Gd, forming the IR783-GK10-BHQ3-Gd probe. Upon MMP-9 cleavage of GK10, BHQ3 is released from the probe, thereby amplifying the previously quenched IR783 fluorescence signal. *In vitro* experiments demonstrate the probe's impressive detection limit for MMP-9, as low as 1.84 ng/mL. Moreover, *in vivo* imaging results reveal that the probe can differentiate liver cancers with varying metastatic capacities. The fluorescence and MR imaging signal intensity of high metastatic HCC are approximately 1.2 times greater than that of low metastatic HCC. Thus, this engineered probe holds promise as a valuable tool for evaluating HCC metastatic capacity through fluorescence-MR dual-mode imaging.

According to the data from the International Agency for Research on Cancer of the World Health Organization, liver cancer claimed the lives of approximately 830,000 individuals globally in 2020 [1]. Liver cancer has become the third leading cause of cancer-related fatalities, posing a severe threat to human life and health [2]. Among the histological subtypes of liver cancer, hepatocellular carcinoma (HCC) is the predominant form, accounting for 90% of primary liver cancer [3,4]. Characterized by insidious onset, rapid progression, and heightened malignancy, HCC results in a 40% to 70% five-year recurrence rate, ultimately leading to a poor prognosis for liver cancer patients [5-7]. Meanwhile, invasion and metastasis are the leading causes of high recurrence and high mortality of HCC [8-10]. Therefore, the development of molecular imaging techniques for visual assessment of the invasiveness and metastatic potential of HCC holds significant importance in guiding clinical treatment strategies for HCC and improving patient prognosis.

A growing body of evidence indicates that using biomarkers or microenvironment changes related to HCC metastasis may offer a more sensitive and practical approach to diagnosis, avoiding frequent radiation exposure [11,12]. Tumor metastasis involves a complex cascade process, with the first stage characterized by invasion [13-15]. During this crucial process, the degradation of extracellular matrix, including the basement membrane, serves as a pivotal starting point [16-18]. Matrix metalloproteinase-9 (MMP-9), a zinc-dependent endopeptidase, plays a direct role in the degradation of collagen, a central component of both extracellular matrix and basement membrane [19,20]. This enzymatic action sets the stage for creating an environment conducive to the invasion and metastasis of HCC. Clinical data suggest that MMP-9 may serve as a potent biomarker associated with invasive metastasis in HCC. Yang *et al.* revealed that the positive expression of MMP-9 is an inde-

* Corresponding authors.
E-mail addresses: renwzh@nimte.ac.cn (W. Ren), aiguo@nimte.ac.cn (A. Wu).
[1] These authors contributed equally to this work.

https://doi.org/10.1016/j.cclet.2024.110212
1001-8417/

pendent factor of poor prognosis of HCC through statistical analysis of tumor resection samples from 129 HCC patients [21]. Wang *et al.* found that Runt-related transcription factor 2 regulates the accumulation of MMP-9 in HCC cells by immunohistochemical staining of hepatocellular carcinoma tissue specimens. They mechanistically demonstrated a positive correlation between the overexpression of MMP-9 and the invasiveness of HCC [22]. Ali *et al.* used a qualitative modeling framework to predict the role of biological regulatory network in the invasion and metastasis of HCC. The results show that the feedback loop of transforming growth factor beta1 and MMP-9 is very important in the invasion and metastasis of HCC [23]. Therefore, designing a specific molecular probe targeting MMP-9 for assessing tumor metastasis is expected to predict HCC prognosis at its early stage.

Fluorescence imaging, as a novel imaging modality, has shown considerable promise in medical imaging due to its non-invasive detection and high sensitivity [24-27]. However, most fluorescent probes operate in a "normally open" mode, which can lead to non-specific false positive signals and reduced imaging efficacy [28-31]. Therefore, constructing "off-on" enzyme-activatable probes based on Förster resonance energy transfer (FRET) signal conversion matrix is beneficial to improve sensitivity and specificity in detection [32-35]. In recent years, various fluorescent probes have been developed to detect MMP-9 in living systems. For instance, Li *et al.* assembled polymer dots linked with MMP-9 recognizable peptides onto graphene oxide surface to prepare GO-Pep-Pdot nanocomposites, successfully detecting MMP-9 in clinical serum samples from prostate cancer patients [36]. Cai *et al.* constructed an MMP-P12 probe by combining near-infrared fluorophore Cy5.5 with a quencher, enabling the dynamic monitoring of MMP-9 changes in diabetic stroke by optical imaging [37]. Similarly, Dadmehr *et al.* utilized the FRET effect between gold nanoparticles and nanoclusters to construct a nanocomposite platform for visual and colorimetric detection of MMP-9 enzyme in human serum [38]. Furthermore, Rainu *et al.* synthesized a dual-responsive fluorescent nanoprobe using carbon nanoparticles and MMP-9 sensitive peptides [39]. This nanoprobe enabled the detection of pH and MMP-9 level changes, effectively distinguishing between cancerous and non-cancerous microenvironments.

However, fluorescence imaging alone cannot provide precise localization information of diseased tissue [33,40,41]. In contrast, magnetic resonance (MR) imaging offers advantages such as ionizing radiation-free imaging, exceptional spatial resolution, and precise structural positioning, making it an excellent tool for liver cancer diagnosis [42-44]. By integrating the advantages of both imaging modalities, designing a probe endowed with dual-mode imaging capabilities of fluorescence and MR imaging could significantly enhance the precise imaging of HCC with different metastatic capacities. However, there is a lack of studies on MMP-9 responsive probes for imaging assessment of HCC metastasis, particularly in the fluorescence-MR dual-mode imaging probes.

In this study, we designed and synthesized an MMP-9-responsive fluorescence-MR dual-mode imaging probe named IR783-GK10-BHQ3-Gd. As illustrated in Scheme 1, the probe was constructed upon the MMP-9 cleavable polypeptide sequence GK10 (GCPLGVRGDK), covalently linked with the near-infrared fluorescent molecule IR783, integrated with quenching group BHQ3 and MR imaging contrast agent DOTA-Gd. MMP-9 can activate the fluorescence signal of the probe. To comprehensively evaluate the probe's capability to detect metastatic HCC, we selected three subtypes of HCC cells with diverse metastatic potentials and established corresponding tumor mouse models. We then assessed the probe's ability to distinguish between high and low metastatic HCC by fluorescent and MR imaging. Our results indicate that the HCC model with the strongest metastasis exhibited a higher fluorescence signal in response to MMP-9. This suggests that the constructed probe holds promise for assessing HCC's metastatic capability through fluorescence-MR dual-mode imaging, thereby potentially guiding the formulation of clinical therapeutic approaches for HCC.

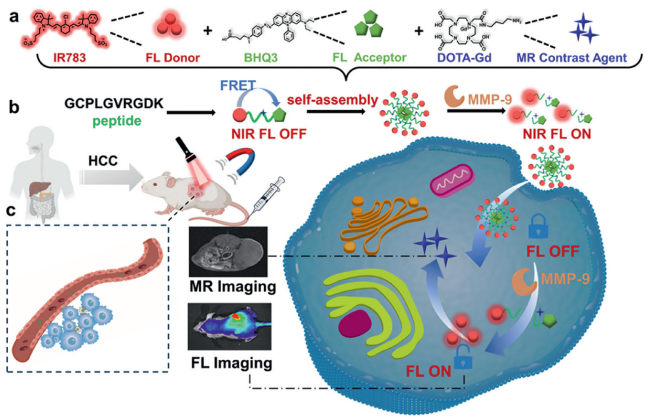

Scheme 1. Diagram of the IR783-GK10-BHQ3-Gd probe synthesis process and its MMP-9 responsive fluorescence and MR dual-mode imaging of HCC models with different metastatic capacities.

The synthetic route of the IR783-GK10-BHQ3-Gd probe is depicted in Fig. S1 (Supporting information). Near-infrared fluorescent molecule IR783 and the corresponding quenching group BHQ3 were labeled at both ends of GCPLGVRGDK, abbreviated as GK10, and DOTA-Gd was modified for MR imaging, resulting in the formation of IR783-GK10-BHQ3-Gd. The purity of the probes was characterized using TOF-MS, as shown in Fig. S2 (Supporting information). The spectral results show that the quasimolecular ion peaks *m/z* 1777.7477, 2262.0517, 631.1787, and 3065.8629 were detected in the positive ion mode of the ESI of the mass spectrometry for IR783-GK10, IR783-GK10-BHQ3, DOTA-Gd, and IR783-GK10-BHQ3-Gd, respectively. These results are consistent with the theoretical signal simulation, confirming the successful synthesis of the IR783-GK10-BHQ3-Gd probe.

Transmission electron microscopy (TEM) images in Fig. 1a show that the probe is spherical. Dynamic light scattering (DLS) data in Fig. 1b reveal that the average hydrodynamic diameter of the probe is 117.5 ± 3 nm, with a polydispersity index PI value of 0.1509. Additionally, as depicted in Fig. 1c, the surface of IR783-GK10-BHQ3-Gd exhibits a negative charge with a potential of −6.624 mV. Collectively, these data suggest that the IR783-GK10-BHQ3-Gd probe exhibits good dispersibility and uniform size. As shown in Fig. S3 (Supporting information), the standard concentration curve of IR783 was established, yielding the standard line equation $y = 0.206x - 0.0312$ by linear fitting, with a correlation coefficient R^2 of 0.9998, indicating good linearity. According to the standard concentration curve of IR783, IR783-GK10, IR783-GK10-BHQ3, and IR783-GK10-BHQ3-Gd concentrations were standardized to IR783 = 5 μg/mL. By comparing the corresponding absorption spectra in Fig. 1d, it is observed that the maximum absorption peak of IR783-GK10-BHQ3-Gd is 791 nm, which is red-shifted by 13 nm compared to that of free IR783. This shift may be attributed to the replacement of chloride ions, causing a disruption of original structure and resulting in a Stokes shift.

Next, the *in vitro* performance of the probe was verified. Figs. 1e and f show T1-weighted magnetic resonance image and relaxation curve. With the increase of Gd^{3+} concentration from 0.02 mmol/L to 0.1 mmol/L, the MR signal becomes stronger. By calculating the relaxation values of different Gd concentrations, the r_1 and r_2 values are 10.033 and 10.842 $(mmol/L)^{-1}$ s^{-1}, respectively, and the r_2/r_1 value is 1.08, which indicates that the probe has good T_1-weighted MR performance.

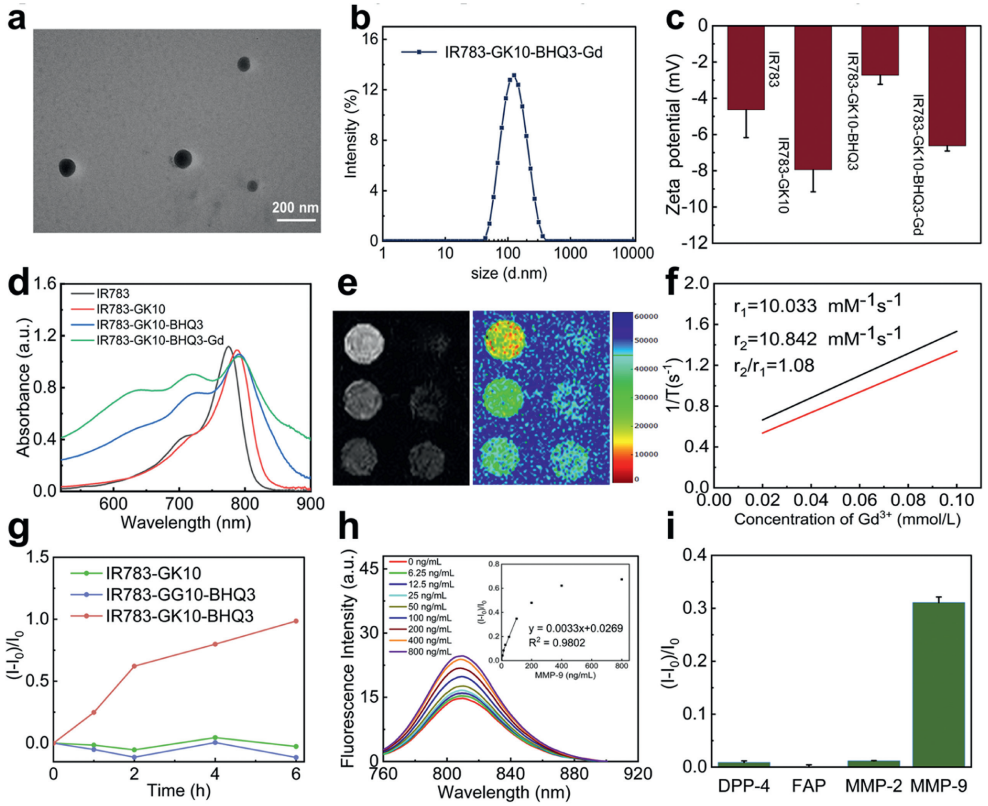

Fig. 1. (a) TEM image of IR 783-GK10-BHQ3-Gd. (b) The distribution of hydrodynamic size of IR 783-GK10-BHQ3-Gd. (c) Zeta potential and (d) UV–vis absorption spectra of IR783, IR783-GK10, IR783-GK10-BHQ3 and IR783-GK10-BHQ3-Gd. (e) T_1-weighted MR imaging and (f) relaxation curve of IR783-GK10-BHQ3-Gd. (g) Fluorescence signal intensity growth rates of IR783-GK10, IR783-GG10-BHQ3, IR783-GK10-BHQ3 incubated with MMP-9 for different times. (h) Fluorescence spectra of IR783-GK10-BHQ3-Gd incubation with different concentrations of MMP-9 (inset: Fluorescence growth rate of IR783-GK10-BHQ3-Gd probe incubated with varies MMP-9 concentration). (i) Fluorescence growth rate $(I-I_0)/I_0$ of the probe incubated with different types of enzymes. All data are presented as mean ± standard deviation (SD) ($n=3$). mM = mmol/L.

To evaluate the enzyme response of the probe *in vitro*, human recombinant MMP-9 was utilized to analyze the enzyme response of the probe, with IR783-GK10 and IR783-GG10-BHQ3 probes as negative controls. Specifically, IR783-GK10 lacks the quencher BHQ3, while IR783-GG10-BHQ3 does not contain the MMP-9 cleavable targeting peptide. The fluorescence intensities of three probes were compared before and after enzyme digestion, and changes in fluorescence growth rates at different time points were calculated.

As shown in Fig. 1g, the fluorescence of the IR783-GK10-BHQ3 probe in the experimental group exhibits a significantly enhancement compared with the control group, with the fluorescence growth rate exceeding 100% after 6 h. Conversely, the fluorescence of the probe in the control group remains nearly zero within 6 h. Fluorescence imaging images collected at different incubation time points (Fig. S4 in Supporting information) demonstrate a notable increase in the fluorescence signal of the IR783-GK10-BHQ3 probe in the experimental group over time.

To further characterize the sensitivity of the probe in detecting MMP-9, the IR783-GK10-BHQ3-Gd probe at concentration of 20 μg/mL was mixed with MMP-9 at concentration ranging from 0 to 800 ng/mL (0, 6.25, 12.5, 25, 50, 100, 200, 400, 800 ng/mL) in enzyme reaction buffer (TCNB buffer, 50 mmol/L Tris, 10 mmol/L $CaCl_2$, 150 mmol/L NaCl, 0.05% Brij-35, pH 7.5) at 37 °C for 2 h. As depicted in Fig. 1h, the fluorescence intensity of the probe after enzyme digestion exhibits a positive correlation with the concentration of MMP-9 before reaching a stable level of 400 ng/mL. When the concentration of MMP-9 is below than 100 ng/mL, a linear relationship between the intensity of activated fluorescence and the concentration of MMP-9 is observed, with $R^2 = 0.9802$. Furthermore, the detection limit was calculated to be 1.84 ng/mL according to the formula $3\sigma/k$, where 3σ is the standard deviation of the blank sample ($n=5$) and k is the slope of the analyte's corresponding linear curve [45].

To evaluate the selectivity of the probe to MMP-9, the IR783-GK10-BHQ3-Gd probe was incubated with different types of enzymes, including dipeptidyl peptidase-4 (DPP-4), fibroblast activating protease (FAP), MMP-2 and MMP-9, under the same conditions of 2 h at 37 °C. The results presented in Fig. 1i demonstrate that MMP-9 effectively activates fluorescence compared with other enzymes. Here, I_0 represents the fluorescence signal intensity before enzyme digestion, while I represents the fluorescence signal intensity after enzyme digestion. These findings collectively confirm the high sensitivity and selectivity of the probe, rendering it suitable for quantitative detection of activated MMP-9 *in vitro* and *in vivo*.

In addition, we measured the stability of the probe in response to MMP-9 in buffers with varying pH levels. The results, presented in Figs. S5 and S6 (Supporting information), indicate that the probe exhibits stable responses to MMP-9 in buffers with pH values of 5.5, 6.5, and 7.4. Therefore, it is estimated that the IR783-GK10-BHQ3-Gd probe can detect MMP-9 under physiological pH conditions.

Before investigating the imaging potential of the probe in HCC cells *in vitro*, we initially evaluated the cytotoxicity of the probe by CCK-8 method. As shown in Fig. S7 (Supporting information), the relative activities of four types of cells, including normal live cells L02 and HCC cells with various metastatic abilities (HepG2, 97L, LM3), all remain above 85% when incubated for 24 h with the probe concentration range of 0–30 μg/mL. Moreover, even at the high probe concentration of 40 μg/mL, the cell survival rate exceeds 80% after 24 h of incubation.

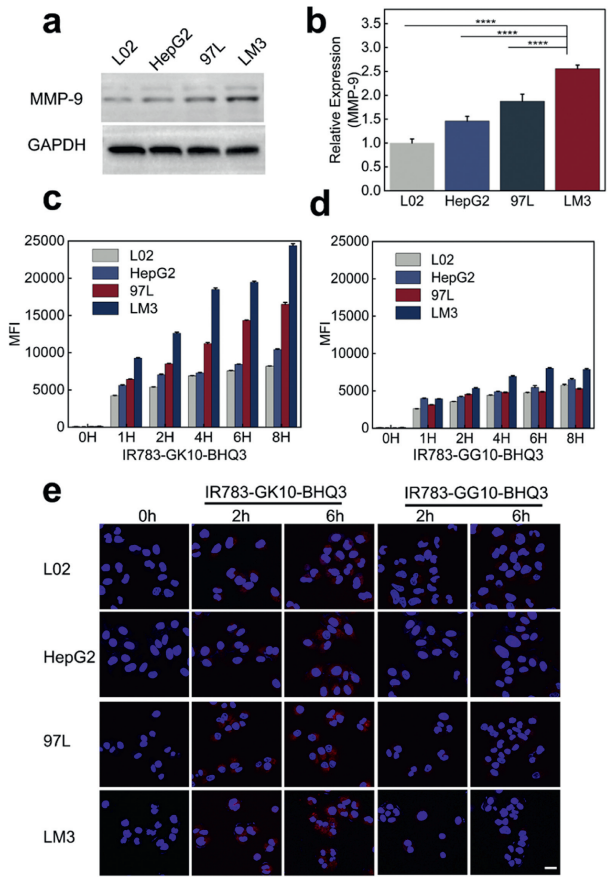

Fig. 2. (a) MMP-9 expression and (b) quantification in normal hepatocyte L02 cells and HCC cells (HepG2, 97L, and LM3). (c) Cellular uptake of IR783-GK10-BHQ3 and (d) IR783-GG10-BHQ3 in L02, HepG2, 97L, and LM3 cells using flow cytometry analysis, as well as (e) laser confocal observation. Scale bar: 25 μm. All data are presented as means ± SD from at least three independent experiments. $^{****}P < 0.0001$. GAPDH, glyceraldehyde 3-phosphate dehydrogenase; MFI, mean fluorescence intensity.

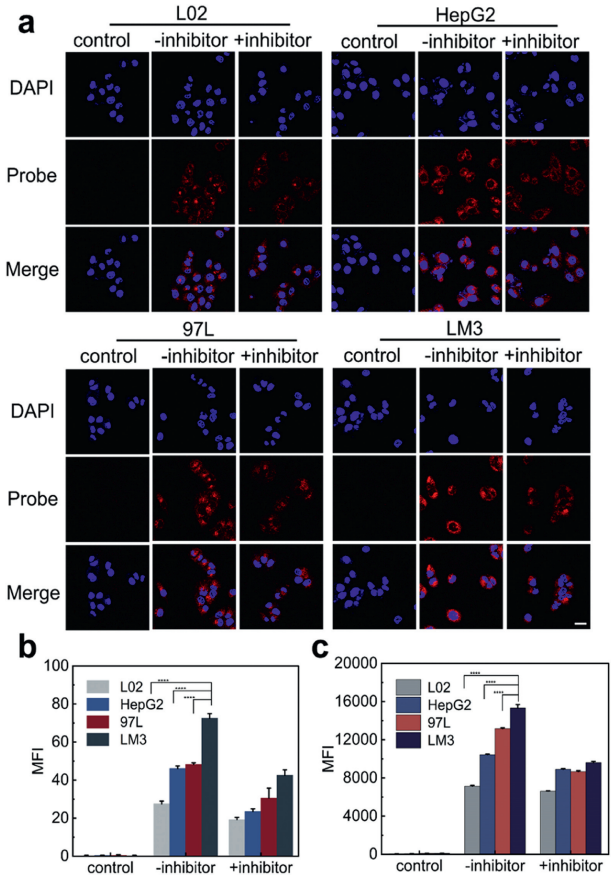

Fig. 3. (a) Laser confocal imaging, (b) its fluorescence quantification, and (c) flow cytometry analysis of the four types of cells incubated with the IR783-GK10-BHQ3-Gd probe with or without the enzyme inhibitor SB-3CT. Scale bar: 25 μm. All data are presented as mean ± SD from at least three independent experiments. $^{****}P < 0.0001$.

Western blot analysis was conducted to compare the MMP-9 expression levels between normal hepatocytes (L02) and HCC cells (HepG2, 97L, LM3). As shown in Figs. 2a and b, MMP-9 expression in HCC cells is significantly elevated compared to that in normal hepatocytes L02. Furthermore, MMP-9 expression in the three types of HCC cells exhibits varying trends depending on their metastatic ability. Specifically, LM3 cells with high metastatic potential exhibits the highest MMP-9 expression levels, which is 2.5 times higher than that of L02 cells, followed by 97L cells, whereas HepG2 cells with the lowest metastatic potential display the lowest levels of MMP-9 expression.

Further, we investigated the uptake ability of four types of cells to the IR783-GK10-BHQ3 probe, and observed the cellular uptake effect of the probe at different time points using flow cytometry, with the IR783-GG10-BHQ3 probe without targeting peptide as the control. As revealed in Figs. 2c and d, the uptake of IR783-GK10-BHQ3 probe by four types of cells is time-dependent. As the incubation time prolongs, the cellular uptake increases, leading to enhanced fluorescence, with LM3 cells exhibiting the highest fluorescence intensity due to their high metastatic ability. In contrast, the control group with the IR783-GG10-BHQ3 probe lacking targeting peptide shows minimal changes in fluorescence intensity over time. Furthermore, we assessed the imaging effects of the two probes in cells by laser confocal images at 2 and 6 h, yielding consistent results as displayed in Fig. 2e. The fluorescence images of the four cells incubated with IR783-GG10-BHQ3 exhibit minimal change at both time points, whereas the IR783-GK10-BHQ3 group shows a noticeable enhancement trend. The fluorescence intensity of LM3 cells is approximately 2.5 times higher compared to that in L02 cells, which interestingly coincides with the MMP-9 expression levels in these two cell lines.

To further verify the positive correlation between the fluorescence effect and MMP-9 content, cells were pretreated with the inhibitor SB-3CT, and then observed using a combination of laser confocal microscope (Figs. 3a and b) and flow cytometry (Fig. 3c). It is found that addition of inhibitor significantly inhibits the fluorescence signal. Upon comparing the fluorescence intensity of different cells, it is noted that normal L02 cells show a lower fluorescence signal compared to HCC cells HepG2, 97L and LM3. Notably, the highly metastatic HCC cells LM3 show higher expression of MMP-9, resulting in the highest fluorescence signal. The above findings collectively indicate that the IR783-GK10-BHQ3-Gd probe can specifically image MMP-9 activity in HCC cells and has the potential to distinguish HCC cells with different metastatic abilities.

To assess the biosafety of the probe, major organs including the heart, liver, spleen, lung and kidney were collected from mice for from the mice for histopathological analysis after drug administration for 14 days. All the animal experiments were carried out under the guideline of the Experimental Animal Ethics Committee of Ningbo University (Permit No. SYXK Zhe 2024-0002). As shown in Figs. S8 and S9 (Supporting information), mice in both groups exhibit uniform weight gain over the 14 days, and no damage to the major organs is observed in either the experimental or control groups, with evident normal cell morphology and without any lesions. Furthermore, we compared the experimental group's

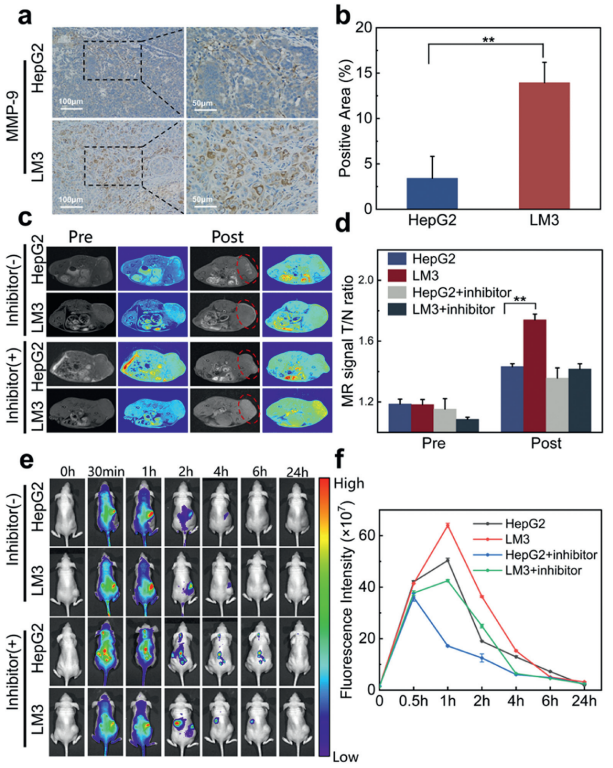

Fig. 4. (a) Immunohistochemical staining and (b) quantification analysis of the MMP-9 expression in HepG2 and LM3 tumor tissues. Scale bar: 100 μm. (c) T_1-weighted MR imaging of HepG2 and LM3 tumor-bearing mice before and after tail vein injection of IR783-GK10-BHQ3-Gd probe (4 mg/kg, 100 μL) with or without inhibitor SB-3CT pretreatment. (d) Quantification of MR signal of tumor in panel c. (e) Fluorescence imaging of tumor-bearing mice at various time points following tail vein injection of IR783-GK10-BHQ3-Gd probe (2 mg/kg, 100 μL) with or without inhibitor SB-3CT pretreatment. (f) Quantification of the tumor fluorescence signal in panel e. All data are presented as means ± SD from at least three independent experiments. $^{**}P < 0.01$.

blood routine and blood biochemical indices with those of healthy mice, revealing no difference in the data between the two groups (Figs. S10 and S11 in Supporting information). The above data collectively indicate that the IR783-GK10-BHQ3-Gd probe has good biosafety and low toxicity.

Subsequently, we evaluated the expression level of MMP-9 in HepG2 and LM3 constructed HCC tumor tissues through immunohistochemically staining. This allowed us to further elucidate the correlation between MMP-9 expression levels and the metastatic potential of HCC. As illustrated in Figs. 4a and b, MMP-9 expression is significantly higher in LM3 group compared to the HepG2 group. This observation aligns with the results from the *in vitro* experiments at cellular level, indicating that the HCC mice with high metastatic potential exhibit elevated MMP-9 expression in tumor site.

To investigate the T_1 contrast efficacy of the IR783-GK10-BHQ3-Gd probe in HCC model mice, MR images were acquired using a 3.0 T clinical MR scanner, as shown in Fig. 4c. The probe was injected *via* the tail vein into two types of tumor-bearing mice, with mice pretreated with enzyme inhibitor SB-3CT serving as the negative control. Fig. 4d shows that after 6 h of probe injection, the MRI signal contrast between tumor and normal tissue is more significant in LM3 mice compared to the HepG2 group, and quantification reveals that tumor to normal (T/N) signal ratio in LM3 is 1.2 times higher than that of the HepG2 group. Notably, the MRI signal ratio of tumor mice is significantly reduced after treatment with inhibitors. These results suggest that the heightened expression of MMP-9 in the tumor site promotes the active targeting of the probe to the tumor area, thereby enhancing the T_1-weighted MR imaging of the tumor site. Consequently, the IR783-GK10-BHQ3-Gd probe emerges as a promising MRI contrast agent.

Finally, to investigate the visualization effect of the probe in HCC mice models with different metastatic capacities, we evaluated its fluorescence imaging performance in mice from 0.5 h to 24 h after intravenous injection. Control experiments were conducted using mice pretreated with the inhibitor SB-3CT. Fluorescence imaging results in Fig. 4e clearly show the tumor's location in the mice, indicating successful delivery of the IR783-GK10-BHQ3-Gd probe to the tumor site following injection into the mice *via* the tail vein. This demonstrates the probe's ability to actively target HCC tissue. Compared to the enzyme inhibitor SB-3CT treatment group, the experimental group's probe exhibits more pronounced fluorescence signals, further confirming the ability of the IR783-GK10-BHQ3-Gd probe to distinguish between MMP-9-positive and MMP-9-negative tissues *in vivo*. Furthermore, quantitative analysis of fluorescence signals at the tumor site (Fig. 4f) reveals that the fluorescence signals of each group reach maximum intensity approximately one hour after injection. Notably, the LM3 group exhibits the strongest fluorescence signals at the tumor site, which is 1.3 times higher than that of the HepG2 group and 1.5 times higher than that of the inhibitor-pretreated group of the same HCC model type.

In conclusion, to further advance the application of probe-based fluorescence-MR dual-mode imaging technology in evaluating the HCC metastasis, this study constructed a cell and tumor mouse model ranging from high to low metastatic ability. We proved the correlation between metastatic capacity and MMP-9 expression. Leveraging this correlation, we designed and synthesized an MMP-9-responsive dual-mode imaging probe, IR783-GK10-BHQ3-Gd. This probe undergoes hydrolysis by MMP-9 overexpressed in HCC cells with high metastatic capacity, disrupting the "FRET" system comprising the near-infrared fluorescent group IR783 and quenching group BHQ3, thereby activating the probe fluorescence. Consequently, the probe can effectively distinguish the positive and negative expression regions of MMP-9, enabling high specificity and high signal-to-noise ratio fluorescence-MR dual-model imaging of HCC models with different metastatic capacity.

Declaration of competing interest

The authors declare that they have no known competing financial interests or personal relationships that could have appeared to influence the work reported in this paper.

CRediT authorship contribution statement

Qiuye Wang: Writing – original draft, Methodology, Investigation, Formal analysis, Data curation, Conceptualization. **Yabing Sun:** Methodology, Formal analysis, Data curation. **Liangxue Lai:** Methodology, Formal analysis, Data curation. **Haijing Cui:** Methodology. **Yonglong Ye:** Methodology. **Ming Yang:** Methodology. **Weihao Zhu:** Methodology. **Bo Yuan:** Methodology. **Quanliang Mao:** Methodology. **Wenzhi Ren:** Writing – review & editing, Supervision, Investigation, Funding acquisition, Conceptualization. **Aiguo Wu:** Supervision, Project administration, Funding acquisition, Conceptualization.

Acknowledgments

This work was financially supported by the National Natural Science Foundation of China (Nos. 32025021, 31971292, 32111540257), the Zhejiang Province Financial Supporting (Nos. 2020C03110 and 2023C04017), the Key Scientific and Technological Special Project of Ningbo City (No. 2020Z094).

Supplementary materials

Supplementary material associated with this article can be found, in the online version, at doi:10.1016/j.cclet.2024.110212.

References

[1] H. Sung, J. Ferlay, R.L. Siegel, et al., CA Cancer J. Clin. 71 (2021) 209–249.
[2] A. Vogel, T. Meyer, G. Sapisochin, et al., Lancet 400 (2022) 1345–1362.
[3] J.M. Llovet, J. Zucman-Rossi, E. Pikarsky, et al., Nat. Rev. Dis. Primers. 2 (2022) 16018.
[4] F. Foerster, S.J. Gairing, S.I. Ilyas, et al., Hepatology 75 (2022) 1604–1626.
[5] J. Bruix, M. Reig, M. Sherman, Gastroenterology 150 (2016) 835–853.
[6] A.B. Benson, M.I. D'Angelica, D.E. Abbott, et al., J. Natl. Compr. Canc. Netw. 19 (2021) 541–565.
[7] T.F. Wen, C. Jin, A. Facciorusso, et al., Hepatobil. Surg. Nutr. 7 (2018) 353–371.
[8] S. Turajlic, C. Swanton, Science 352 (2016) 169–175.
[9] Y.C. Chu, T. Sun, C. Jiang, Chin. Chem. Lett. 33 (2022) 4157–4168.
[10] C.M. Wong, C.C.L. Wong, J.M.F. Lee, et al., Hepatology 55 (2012) 1453–1461.
[11] Y. Wen, N. Jing, M. Zhang, et al., Adv. Sci. 10 (2023) 2206681.
[12] Y.X. Lu, J.J. Xu, Z.Y. Jia, et al., Chin. Chem. Lett. 33 (2022) 1589–1594.
[13] S. Gerstberger, Q.W. Jiang, K. Ganesh, Cell 186 (2023) 1564–1579.
[14] Y.L. Lin, Y. Li, Genes Dis. 7 (2020) 336–350.
[15] A.W. Lambert, D.R. Pattabiraman, R.A. Weinberg, Cell 168 (2017) 670–691.
[16] M.W. Pickup, J.K. Mouw, V.M. Weaver, Embo Rep. 15 (2014) 1243–1253.
[17] F. Kai, A.P. Drain, V.M. Weaver, Dev. Cell 49 (2019) 332–346.
[18] A.D. Theocharis, S.S. Skandalis, C. Gialeli, et al., Adv. Drug Deliv. Rev. 97 (2016) 4–27.
[19] A.R. Farina, A.R. Mackay, Cancers 6 (2014) 240–296.
[20] H. Huang, Sensors 18 (2018) 3249.
[21] P. Yang, W.J. Yuan, J.T. He, et al., Hepatol. Res. 39 (2009) 1169–1177.
[22] Q. Wang, W. Yu, T. Huang, et al., Oncol. Rep. 36 (2016) 2777–2784.
[23] S. Tariq Ashraf, A. Obaid, M. Tariq Saeed, et al., Math. Biosci. Eng. 16 (2019) 3285–3310.
[24] S. Bouccara, G. Sitbon, A. Fragola, et al., Curr. Opin. Biotechnol. 34 (2015) 65–72.
[25] T. Imamura, T. Saitou, R. Kawakami, Cancer Sci. 109 (2018) 912–918.
[26] S.G. Hou, L. Liang, S.H. Deng, et al., Sci. China Chem. 57 (2014) 100–106.
[27] R.Q. Yang, K.L. Lou, P.Y. Wang, et al., Small Method. 5 (2021) 2001066.
[28] E. Lacivita, M. Leopoldo, F. Berardi, et al., Curr. Med. Chem. 19 (2012) 4731–4741.
[29] P.C. Zhang, A.G. Cheetham, L.L. Lock, et al., Curr. Opin. Biotech. 34 (2015) 171–179.
[30] X.Q. Chen, Y.N. Bian, M.R. Li, et al., Chem. Asia J. 15 (2020) 3983–3994.
[31] J.J. Li, F.F. Cheng, H.P. Huang, et al., Chem. Soc. Rev. 44 (2015) 7855–7880.
[32] X.F. Wu, R. Wang, N. Kwon, et al., Chem. Soc. Rev. 51 (2022) 450–463.
[33] Y.Q. Wang, Y.X. Hu, D.J. Ye, Angew. Chem. Int. Ed. 61 (2022) e202209512.
[34] Y.X. Li, D.T. Xie, Y.X. Yang, et al., Molecules 27 (2022) 4501.
[35] H.W. Liu, L.L. Chen, C.Y. Xu, et al., Chem. Soc. Rev. 47 (2018) 7140–7180.
[36] Q.Y. Li, Y.L. Wang, G.P. Yu, et al., Nanoscale 11 (2019) 20903–20909.
[37] Y. Cai, S. Leng, Y.Y. Ma, et al., Biomater. Sci. 9 (2021) 2562–2570.
[38] M. Dadmehr, M. Mortezaei, B. Korouzhdehi, Biosens. Bioelectron. 220 (2023) 11489.
[39] S. Rainu, S. Parameswaran, S. Krishnakumar, N. Singh, J. Mater. Chem. B 10 (2022) 5388–5401.
[40] Z.T. Rosenkrans, C.A. Ferreira, D.L. Ni, W.B. Cai, Adv. Healthc. Mater. 10 (2021) 2000690.
[41] S.Y. Lee, S.I. Jeon, S. Jung, et al., Adv. Drug Deliv. Rev. 76 (2014) 60–78.
[42] Y.Y. Kim, M.S. Park, K.S. Aljoqiman, et al., Clin. Mol. Hepatol. 25 (2019) 223–233.
[43] J.D. Gordan, E.B. Kennedy, G.K. Abou-Alfa, et al., J. Clin. Oncol. 38 (2020) 4317–4345.
[44] D.X. Zhao, J. Cao, L. Zhang, et al., Biosensors 12 (2022) 342.
[45] F. Qu, Z. Wang, C. Li, D.F. Jiang, X.E. Zhao, Sens. Actuat. B: Chem. 359 (2022) 131610.